Available online at www.sciencedirect.com
ScienceDirect
Journal of Sound and Vibration 299 (2007) 540–558
JOURNAL OF SOUND AND VIBRATION
www.elsevier.com/locate/jsvi

Vibration analysis of drillstrings with self-excited stick–slip oscillations

Y.A. Khulief*, F.A. Al-Sulaiman, S. Bashmal

Department of Mechanical Engineering, King Fahd University of Petroleum and Minerals, KFUPM Box 1767, Dhahran 31261, Saudi Arabia

Received 11 July 2005; received in revised form 16 June 2006; accepted 19 June 2006
Available online 2 October 2006

Abstract

Drillstring vibration is one of the major causes for a deteriorated drilling performance. Field experience revealed that it is crucial to understand the complex vibrational mechanisms experienced by a drilling system in order to better control its functional operation and improve its performance. Sick–slip oscillations due to contact between the drilling bit and formation is known to excite severe torsional and axial vibrations in the drillstring. A dynamic model of the drillstring including the drillpipes and drillcollars is formulated. The equation of motion of the rotating drillstring is derived using Lagrangian approach in conjunction with the finite element method. The model accounts for the torsional–bending inertia coupling and the axial–bending geometric nonlinear coupling. In addition, the model accounts for the gyroscopic effect, the effect of the gravitational force field, and the stick–slip interaction forces. Explicit expressions of the finite element coefficient matrices are derived using a consistent mass formulation. The generalized eigenvalue problem is solved to determine modal transformations, which are invoked to obtain the reduced-order modal form of the dynamic equations. The developed model is integrated into a computational scheme to calculate time-response of the drillstring system in the presence of stick–slip excitations.

1. Introduction

The problem of drillstring vibrations has been recognized for many years as one of the prime causes of deterioration in drilling performance, and was subjected to some early investigations as reported in the literature [1–5]. Field observations based on downhole and surface vibration measurements have indicated that drillstrings exhibit severe vibrations. These vibrations are observed to become more severe at the bottom hole assembly (BHA). The BHA refers to the lower part of the drillstring, which normally includes the drillcollars, stabilizers and the bit, as indicated in Fig. 1. The main reasons for drillstring vibrations are due to contact of the bit with the formation and contact of the drillstring (drill pipe, drill collars and stabilizers) with the borehole. Bent pipes and misalignment of the drillstring represent additional causes for drillstring vibrations. Such vibrations, in general, consist of axial, flexural and torsional deformations [3]. However, stick–slip is considered as the most detrimental type of torsional vibration to the service life of the drillstring

*Corresponding author.
E-mail address: khulief@kfupm.edu.sa (Y.A. Khulief).

0022-460X/$ - see front matter © 2006 Elsevier Ltd. All rights reserved.
doi:10.1016/j.jsv.2006.06.065

Nomenclature

A	cross-sectional area
$\mathbf{e}$	vector of nodal coordinate
E	modulus of elasticity
f	frequency of bit oscillations
G	shear modulus
$\mathbf{G}$	gyroscopic matrix
I_D	diameteral mass moment of inertia
I_P	polar mass moment of inertia
$\mathbf{K}$	global stiffness matrix
$\mathbf{k}_a$	axial stiffness matrix
$\mathbf{k}_{as}$	axial stiffening matrix
$\mathbf{k}_b$	bending stiffness matrix
$\mathbf{k}_\phi$	torsional stiffness matrix
l	length of the finite element
$\mathbf{M}$	global mass matrix
$\mathbf{M}_e$	torsional–lateral coupling mass matrix
$\mathbf{M}_r$	rotary inertia mass matrix
$\mathbf{M}_t$	translational mass matrix
$\mathbf{M}_\phi$	torsional mass matrix
$\mathbf{N}_t$	translational shape function
$\mathbf{N}_\phi$	torsional shape function
$\mathbf{N}_\theta$	rotational shape function
t	time
T	kinetic energy
U	total strain energy of drillstring element
U_e	elastic strain energy
U_s	strain energy due to axial stiffening
U_1	strain energy-axial deformation
U_2	strain energy-torsional deformation
U_3	strain energy-bending deformation
W_0	mean weight on bit
φ	angular displacement of bit $= 2\pi ft$
ϕ	elastic rotational deformation
μ_k	kinetic friction coefficient
ρ	density of drillstring material
θ_y	lateral deflection in y-direction
θ_z	lateral deflection in z-direction
$\boldsymbol{\omega}$	instantaneous angular velocity vector
BHA	bottom hole assembly
RPM	revolutions per minute (rev/min)
TOB	torque-on-bit
WOB	weight-on-bit

and downhole equipment. Successive stick–slip oscillations induce large cyclic stresses, which can lead to fatigue problems, reduction of bit life, unexpected changes in drilling direction, and may even result in failure of the drillstring.

Several dynamic formulations have been reported for investigating specific aspects of drillstring vibrational behavior. A few investigations tackled the stick–slip aspect in drilling systems. One of the major difficulties in modeling stick–slip arises from the inaccurate description of some involved parameters and downhole boundary conditions. Moreover, the analysis of the stick–slip phenomenon is numerically challenging, because the static and kinetic friction mechanisms normally result in discontinuities in the dynamic model [6]. However, most of the reported stick–slip investigations have attributed the associated oscillations to static friction effects resulting from rock/bit interaction [7–9]. A few models of drillstring stick–slip were based on a single degree of freedom torsional pendulum [10–15], wherein a rigid body with constant mass and moment of inertia was used to model the BHA and a linear spring to model the drillstring. Richard and Detournay [14,15] adopted a simple torsional spring to model the drillpipe with a lumped mass and inertia to model the BHA. The stick–slip model was based on two processes; namely cutting and friction for an idealized drag bit with an identical set of radial blades. The forces associated with the cutting process are taken to be proportional to the depth of cut, while the frictional forces depend on a rate-independent friction coefficient. Most often, the friction is taken as a non-linear function and is fitted using field data [12,16,17]. Leine et al. [18] addressed the combined torsional (stick–slip) and lateral (whirling) vibrations. They used a low-dimensional model to describe the stick–slip whirl interaction. The BHA was modeled as a rigid disk at the end of a massless flexible drillpipe.

Although, such simple models provided some insight into this complex phenomenon, they ignored the continuum nature of the drillstring. In order to capture the multi-degree of freedom elastic behavior of the drillstring, some higher-order models were introduced. Yigit and Christoforou [19,20] presented dynamic models of a rotating drillstring based on the Lagrangean formulation and the assumed modes method. One model accounts for the coupling between axial and transverse vibrations, and the other accounts for the coupling between torsional and transverse vibrations. The effect of the gravitational field on the drillstring dynamics was addressed by Tucker and Wang [21] in modeling the integrated drillstring assembly. They

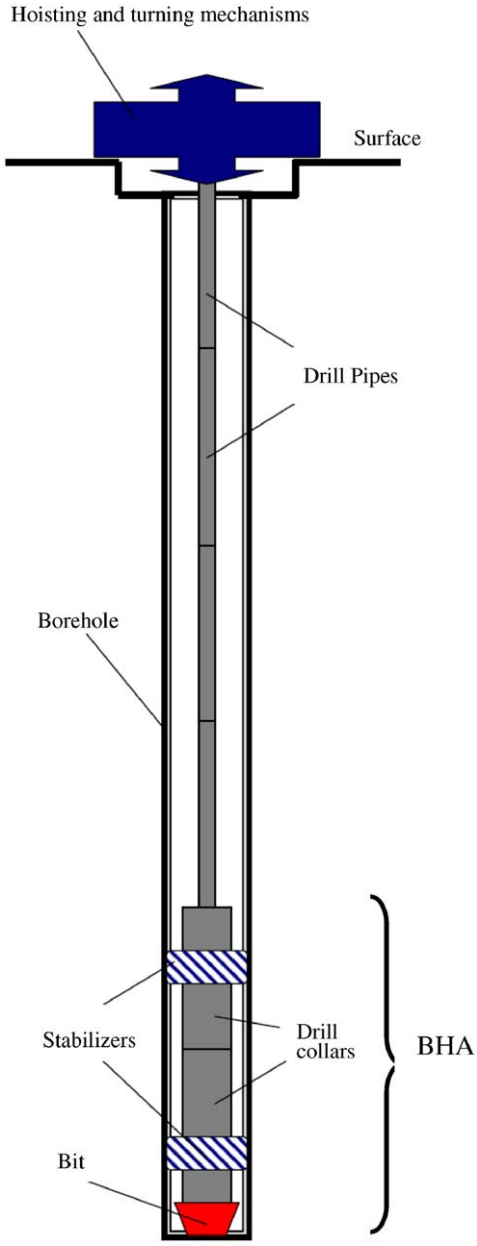

Fig. 1. A typical drillstring configuration.

viewed the special nature of the drillstring structure as elastic space curves, and presented an analytical model based on the one-dimensional (1D) Cosserat continua, wherein the BHA was modeled as point mass with rotary inertia attached to the end of drillstring.

The finite element technique has been recognized as one the most practical methods for the analysis of large-scale structures. Several studies have been carried out to capture the complexity of drillstring motion using the finite element method. One of the early attempts to use the finite element method in drillstring analysis was reported by Millheim et al. [22]. Their work was dedicated to modeling the BHA by utilizing a general purpose finite element program. Other finite element analyses dedicated to studying the BHA followed [23–27]. These investigations focused on evaluating modal characteristics, performing harmonic analyses or evaluating

mechanical properties of a non-rotating BHA. In all such models, the drillstring rotation was not considered. Apostal et al. [27] developed a finite element model to study the forced frequency response of a non-rotating BHA using the lumped mass approach, wherein the damping effect was included. Apostal et al. [27] presented a finite element model of the BHA, wherein they demonstrated that effect of damping can be augmented to a FEM model used for forced frequency response analysis. Axisa and Antunes [28] presented a dynamic modeling scheme using the finite element method. The model included both flexural and torsional motions, which were treated as uncoupled. The formulation did not address the gyroscopic and gravitational axial stiffening effects. Dunayevsky et al. [29] employed the finite element to calculate the modal characteristics of the drillstring for the purpose of instability analysis. The gyroscopic effect and the axial stiffening due to the gravitational field were not included in that model. Berlioz et al. [30] applied the rotordynamics theory together with the finite element method to derive a dynamic model for the drillstring. A two-node finite shaft element was used with six DOF per node. Although the model accounts for the gyroscopic and fluidelastic effects, the axial stiffening associated with the tension and compression segments of the drillstring was not included in their equations. Recently, Melakhessou et al. [31] utilized the FEM code developed in Ref. [30] to determine only the contact zone in their drillstring/contact study. Yet, the drillstring was modeled as an unbalanced rotor supported by two bearings. The proposed mathematical model is expressed in terms of four independent degrees of freedom which are radial displacement, rotation of the section considered, bending along the tangential direction and torsion of the string. The nonlinear equations of motion are derived using Lagrange equations and are solved numerically to obtain the response. However, the stick–slip excitation was not considered within the framework of the aforementioned finite element models.

With the exception of the work reported by Schmalhorst and Baumgart [32], no other models, which addressed stick–slip motion in conjunction with the finite element modeling of drillstrings, could be cited in the available literature. In Ref. [32], a finite element model was developed to simulate whirl and stick–slip phenomenon. The friction force is treated as being dependent on the contact velocity. However, the axial degrees of freedom and full coupling between structural vibrations were not included in the analysis. The gravitational effects were taken as distributed external forces, and the coefficient of friction was assumed as a function of lateral and torsional velocities, which was defined by some characteristics curve.

It is noted that most of the reported studies focused on modeling the BHA segment of the drillstring. Although there exists an extensive literature devoted to the analysis of distinct aspects of the dynamics of the drillstring and BHA, it is only recently that the virtues of treating the drilling assembly as an integrated system have been considered [33]. The finite element method was only conveniently utilized to model drillstrings, yet the reported models have either addressed the BHA only, or considered the drillstring as a rotating shaft similar to that treated in rotordynamics.

This paper presents a finite element model of the whole elastic drillstring including both drillpipes and drillcollars. In addition to the gyroscopic effect, axial–bending coupling, and the torsional–bending inertia coupling, the developed model accounts for the gravitational stiffening effect and the associated tension and compression fields within the drillstring. The formulation admits modeling of stick–slip self-excited oscillations. A computational scheme is established to integrate equations of motion and to solve for the transient vibration response of drillstring due to different field excitations. The developed model is intended to furnish the basic building block for further development of a more comprehensive model of the drilling assembly as an integrated system that can easily accommodate other related dynamic effects resulting from wellbore/drillpipe contact, drillstring/mudflow interaction, and directional drilling.

2. The elastodynamic model

In this formulation, it is assumed that the material of the drillstring is elastic, homogeneous and isotropic. The deflection of the drillstring is produced by the displacement of points of the centerline. It is further assumed that internal damping and flow-induced forces are neglected at this stage. The finite element method is used to model the drillstring used in rotational vertical drilling operations.

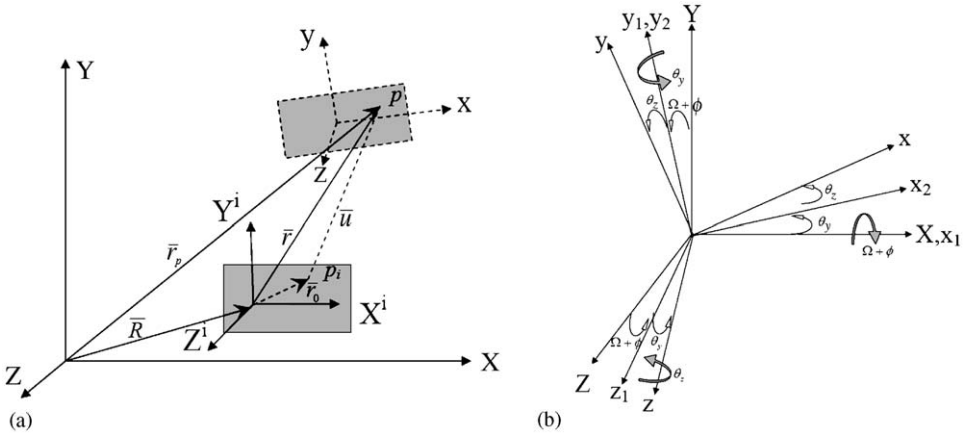

Fig. 2. (a) Element coordinates and (b) elemental cross-section rotational angles.

2.1. Kinetic energy of the finite drillstring element

Referring to Fig. 2, let p be any point in the undeformed shaft element. Point p is defined by the vector $\mathbf{r}_p$ with respect to XYZ global coordinate system. The global position of point p in Fig. 2(a) can be expressed as

$$\mathbf{r}_p = \mathbf{R} + \mathbf{r}_o + \mathbf{u}, \tag{1}$$

where $\mathbf{r}_o$ is the undeformed position and $\mathbf{u}$ represent the deformation vector of point p. Here, $X^iY^iZ^i$ refers to the elemental coordinated system at the undeformed state, while xyz is the elemental coordinate system after deformation. Referring to Fig. 2(b), the xyz coordinate system is related to the $X^iY^iZ^i$ coordinate system through a set of angles ϕ, θ_y and θ_z. To achieve the orientation of any cross-section of the element, the element is first rotated by an angle $(\Omega+\phi)$ about the X^i axis, followed by an angle θ_y about the new y-axis, and finally by an angle θ_y about the final z-axis. The instantaneous angular velocity vector $\boldsymbol{\omega}$ of the xyz frame may be expressed as

$$\boldsymbol{\omega} = (\dot{\Omega}+\dot{\phi})\hat{\mathbf{I}} + (\dot{\theta}_y)\hat{\mathbf{j}}_1 + (\dot{\theta}_z)\hat{\mathbf{k}}_2, \tag{2}$$

where $\hat{\mathbf{I}}$, $\hat{\mathbf{j}}_1$ and $\hat{\mathbf{k}}_2$ are unit vectors along the X, y_1 and z_2 axes, respectively. The term $\dot{\Omega}$ is the constant angular velocity of the rotary table. Transforming Eq. (2) into xyz coordinate and utilizing the linear approximation for the small angles θ_y and θ_y, one can, after some manipulations, express Eq. (2) in the following form:

$$\boldsymbol{\omega} = \begin{Bmatrix} \omega_x \\ \omega_y \\ \omega_z \end{Bmatrix} = \begin{Bmatrix} \dot{\Omega}+\dot{\phi}-\dot{\theta}_z\theta_y \\ \dot{\theta}_y\cos(\Omega+\phi)-\dot{\theta}_z\sin(\Omega+\phi) \\ \dot{\theta}_y\sin(\Omega+\phi)+\dot{\theta}_z\cos(\Omega+\phi) \end{Bmatrix}. \tag{3}$$

Since there is no change in $\mathbf{R}$ and $\mathbf{r}_o$ when the element deforms, one can use the finite element notations to express the vector $\mathbf{u}$ as

$$\mathbf{u} = \mathbf{N}\mathbf{e}, \tag{4}$$

where $\mathbf{N}$ is the shape function matrix of the 3D finite beam element formulation, and $\mathbf{e}$ is the vector of nodal coordinates of the two-node finite string element, which is defined by

$$\mathbf{e} = \{u_1 \quad v_1 \quad w_1 \quad \theta_{y_1} \quad \theta_{z_1} \quad \phi_1 \quad u_2 \quad v_2 \quad w_2 \quad \theta_{y_2} \quad \theta_{z_2} \quad \phi_2\}^{\mathrm{T}}. \tag{5}$$

Utilizing the assumed displacement field, the translational deformations of an element is represented in terms of shape functions as

$$\begin{Bmatrix} u(x,t) \\ v(x,t) \\ w(x,t) \end{Bmatrix} = \begin{bmatrix} N_{u_1} & 0 & 0 & 0 & 0 & 0 & N_{u_2} & 0 & 0 & 0 & 0 & 0 \\ 0 & N_{v_1} & 0 & 0 & N_{v_2} & 0 & 0 & N_{v_3} & 0 & 0 & N_{v_4} & 0 \\ 0 & 0 & N_{v_1} & N_{v_2} & 0 & 0 & 0 & 0 & N_{v_3} & -N_{v_4} & 0 & 0 \end{bmatrix} \mathbf{e}$$
$$= \begin{bmatrix} N_u \\ N_v \\ N_w \end{bmatrix} \mathbf{e} = \mathbf{N}_t(x)\mathbf{e}. \tag{6}$$

The elastic rotation of a typical cross section of the element is then approximated by

$$\begin{Bmatrix} \theta_y \\ \theta_z \end{Bmatrix} = \begin{bmatrix} 0 & N_{\theta_1} & 0 & 0 & N_{\theta_2} & 0 & 0 & N_{\theta_3} & 0 & 0 & N_{\theta_4} & 0 \\ 0 & 0 & -N_{\theta_1} & N_{\theta_2} & 0 & 0 & 0 & 0 & -N_{\theta_3} & N_{\theta_4} & 0 & 0 \end{bmatrix} \mathbf{e}$$
$$= \begin{bmatrix} N_{\theta_y} \\ N_{\theta_z} \end{bmatrix} \mathbf{e} = \left[N_\theta(x)\right]\mathbf{e} \tag{7}$$

and for the torsional deformation of a typical cross section in the form

$$\varphi(x,t) = \begin{bmatrix} 0 & 0 & 0 & 0 & 0 & N_{\varphi_1} & 0 & 0 & 0 & 0 & 0 & N_{\varphi_2} \end{bmatrix} \mathbf{e}$$
$$= \left[N_\varphi\right]\mathbf{e}. \tag{8}$$

Utilizing the time derivative of Eq. (4), the kinetic energy expression can be written as

$$T = \frac{1}{2}\int_V \rho\left(\dot{\mathbf{e}}^{\mathrm{T}}\mathbf{N}_t^{\mathrm{T}}\mathbf{N}_t\dot{\mathbf{e}} + \dot{\mathbf{e}}^{\mathrm{T}}\mathbf{N}_t^{\mathrm{T}}\tilde{\boldsymbol{\omega}}\,\mathbf{r}_p + r_p^{\mathrm{T}}\tilde{\boldsymbol{\omega}}^{\mathrm{T}}\mathbf{N}_t + \mathbf{r}_p^{\mathrm{T}}\tilde{\boldsymbol{\omega}}^{\mathrm{T}}\tilde{\boldsymbol{\omega}}\,\mathbf{r}_p\right)\mathrm{d}V, \tag{9}$$

where ρ is the mass density and the matrix $\tilde{\boldsymbol{\omega}}$ is the (3×3) skew-symmetric matrix associated with the rotational vector $\boldsymbol{\omega}$. The second and third terms in Eq. (9) are identically zero, because the moments of inertia are calculated with respect to the center of mass of the element. The first term represents the kinetic energy due to translation and the last term represents the kinetic energy due to rotational effects that include gyroscopic moments. Upon evaluating the first and last terms, Eq. (9) can be expressed in the form

$$T = \frac{1}{2}\dot{\mathbf{e}}^{\mathrm{T}}\mathbf{M}_t\dot{\mathbf{e}} + \frac{1}{2}C\dot{\boldsymbol{\Omega}}^2 + \frac{1}{2}\dot{\mathbf{e}}^{\mathrm{T}}\mathbf{M}_\varphi\dot{\mathbf{e}} - \dot{\mathbf{e}}\dot{\boldsymbol{\Omega}}^{\mathrm{T}}\mathbf{G}\mathbf{e} - \dot{\mathbf{e}}^{\mathrm{T}}\mathbf{M}_e\dot{\mathbf{e}} + \frac{1}{2}\dot{\mathbf{e}}^{\mathrm{T}}\mathbf{M}_r\dot{\mathbf{e}} = \frac{1}{2}\dot{\mathbf{e}}^{\mathrm{T}}\mathbf{M}\dot{\mathbf{e}} + \frac{1}{2}C\dot{\boldsymbol{\Omega}}^2 - \dot{\boldsymbol{\Omega}}\dot{\mathbf{e}}^{\mathrm{T}}\mathbf{G}\dot{\mathbf{e}}, \tag{10}$$

where $\mathbf{M} = \mathbf{M}_t + \mathbf{M}_r + \mathbf{M}_\varphi - 2\mathbf{M}_e$ is the augmented mass matrix with the constituent matrices given by $\mathbf{M}_t$ as the translational mass matrix, $\mathbf{M}_r$ as the rotary inertia mass matrix, $\mathbf{M}_\varphi$ as the torsional mass matrix, and $\mathbf{M}_e$ as the torsional–transverse inertia coupling mass matrix, which is time dependent. The matrix $\mathbf{G}$ is the gyroscopic matrix. Introducing the designations $\rho I_y = \rho I_y = I_D$, and $\rho I_x = I_p$, one can write the coefficients and expressions for the constituent matrices in Eq. (10) as

$$C = \int_0^l I_p\,\mathrm{d}x, \quad \mathbf{M}_t = \int_0^l \mathbf{N}_v^{\mathrm{T}}\rho A\mathbf{N}_v\,\mathrm{d}x, \quad \mathbf{M}_r = \int_0^l \mathbf{N}_\theta^{\mathrm{T}} I_D\mathbf{N}_\theta\,\mathrm{d}x,$$
$$\mathbf{M}_\varphi = \int_0^l \mathbf{N}_\varphi^{\mathrm{T}} I_p\mathbf{N}_\varphi\,\mathrm{d}x, \quad \mathbf{G} = \mathbf{G}^* - \mathbf{G}^{*\mathrm{T}}, \quad \mathbf{G}^* = \int_0^l I_p\mathbf{N}_{\theta_y}^{\mathrm{T}}\mathbf{N}_{\theta_z}^{\mathrm{T}}\,\mathrm{d}x,$$
$$\mathbf{M}_e = \int_0^l I_p(\mathbf{N}_\varphi^{\mathrm{T}}\mathbf{N}_{\theta_z} e\mathbf{N}_{\theta_y} - \mathbf{N}_\varphi^{\mathrm{T}}\mathbf{N}_{\theta_y}\mathbf{e}\mathbf{N}_{\theta_z})\,\mathrm{d}x.$$

Explicit expressions of the above constituent matrices have been derived and utilized by the computational scheme.

2.2. Strain energy of the finite drillstring element

Recalling that the elastic coordinates consist of three translational deformations (u, v, w), referring to axial and bending, and three rotations (θ_y, θ_z, φ), which are related to bending and torsional deformations. The elastic strain energy term is designated by $U_e = U_1 + U_2 + U_3$, which accounts for axial U_1, torsional U_2 and bending U_3 deformations.

To evaluate the strain energy due to axial deformations, the axial displacement field is defined to account for the effect of large bending deflection on the axial movement. Therefore, the strain in the axial direction can be defined by Eulerian strain tensor as

$$\varepsilon = \frac{\mathrm{d}u}{\mathrm{d}x} - \frac{1}{2}\left[\left(\frac{\mathrm{d}u}{\mathrm{d}x}\right)^2 + \left(\frac{\mathrm{d}v}{\mathrm{d}x}\right)^2 + \left(\frac{\mathrm{d}w}{\mathrm{d}x}\right)^2\right]. \tag{11}$$

The first term in Eq. (11) is the linear term of axial strain, which generates the linear terms in the stiffness matrix. The remaining terms are, which are second-order terms, are usually neglected in linear structural analysis. Upon expansion of the strain energy expression and neglecting higher-order terms, the axial strain energy is obtained as

$$U_1 = \frac{1}{2}EA\int_0^l \left\{\left(\frac{\mathrm{d}u}{\mathrm{d}x}\right)^2 - \left(\frac{\mathrm{d}u}{\mathrm{d}x}\right)^3 - \frac{\mathrm{d}u}{\mathrm{d}x}\left(\frac{\mathrm{d}v}{\mathrm{d}x}\right)^2 - \frac{\mathrm{d}u}{\mathrm{d}x}\left(\frac{\mathrm{d}w}{\mathrm{d}x}\right)^2\right\}\mathrm{d}x. \tag{12}$$

Eq. (12) can be written in matrix form using the finite element deformation coordinates stated previously as

$$\begin{aligned} U_1 = \frac{1}{2}EA\int_0^l \{&\mathbf{e}^{\mathrm{T}}\mathbf{B}_u^{\mathrm{T}}\mathbf{B}_u\mathbf{e} - \mathbf{e}^{\mathrm{T}}\mathbf{B}_u^{\mathrm{T}}\mathbf{B}_u\mathbf{e}\mathbf{B}_u\mathbf{e} \\ &-\mathbf{e}^{\mathrm{T}}\mathbf{B}_u^{\mathrm{T}}\mathbf{N}_{\theta_y}\mathbf{e}\mathbf{N}_{\theta_y}\mathbf{e} - \mathbf{e}^{\mathrm{T}}\mathbf{B}_u^{\mathrm{T}}\mathbf{N}_{\theta_z}\mathbf{e}\mathbf{N}_{\theta_z}\mathbf{e}\}\,\mathrm{d}x. \end{aligned} \tag{13}$$

The other two elastic strain energy terms U_2 and U_3, which represent torsional and bending deformations, respectively, are similar to those derived form Euler's beam theory. Now, the total strain energy can be expressed as $U = U_e + U_s$, where U_s represents the axial stiffening effect due to the gravitational force field. The term U_s can be represented in the form

$$U_s = \frac{1}{2}\int_0^l EA\frac{\partial u}{\partial x}\left(\left(\frac{\partial w}{\partial x}\right)^2 + \left(\frac{\partial v}{\partial x}\right)^2\right)\mathrm{d}x. \tag{14}$$

In this case, the term $EA\,\partial u/\partial x$ represents the gravitation force [34]. Designating the gravitational force by $F(x)$, we can write Eq. (14) in the form

$$U_s = \frac{1}{2}\int_0^l F(x)\left(\left(\frac{\partial w}{\partial x}\right)^2 + \left(\frac{\partial v}{\partial x}\right)^2\right)\mathrm{d}x. \tag{15}$$

It is known that the drillpipe is normally a very long segment of the drillstring, which has a low resistance to any applied axial loads and tend to fail by buckling when subjected to axial compression load. Therefore, drillpipe generally operates under tension load by being suspended at the drive end of the drilling rig at the surface. The BHA of the drillstring, which may include the drillcollar segment, carries some of the drillstring weight, thus becoming under compression in order to generate the cutting force or weight-on-bit (WOB). The point separating the tension and compression fields is called the neutral point, which is defined as the point having zero axial force. In this regard, two gravitational force fields exist within the drillstring; a tension field and a compression field. The gravitational force by $F(x)$ is defined for the two separate fields, accordingly. The details of derivation of $F(x)$ for each force field are presented in Ref. [35].

Upon considering the symmetry of cross-section, i.e., $I_y = I_z = I(x)$, the total strain energy $U = U_e + U_s$ can be expressed as

$$U = \frac{1}{2}EA\int_o^l \left\{ \left(\frac{\mathrm{d}u}{\mathrm{d}x}\right)^2 - \left(\frac{\mathrm{d}u}{\mathrm{d}x}\right)^3 - \frac{\mathrm{d}u}{\mathrm{d}x}\left(\frac{\mathrm{d}v}{\mathrm{d}x}\right)^2 - \frac{\mathrm{d}u}{\mathrm{d}x}\left(\frac{\mathrm{d}w}{\mathrm{d}x}\right)^2 \right\} \mathrm{d}x + \frac{1}{2}EA\int_o^l GI_p\left(\frac{\partial\varphi}{\partial x}\right)^2 \mathrm{d}x + \frac{E}{2}\int_o^l \left\{ I(x)\left[\left(\frac{\partial\theta_y}{\mathrm{d}x}\right)^2 - \left(\frac{\partial\theta_z}{\mathrm{d}x}\right)^2\right]\right\} \mathrm{d}x + \frac{1}{2}\int_o^l F(x)\left[\left(\frac{\partial w}{\mathrm{d}x}\right)^2 + \left(\frac{\partial v}{\mathrm{d}x}\right)^2\right] \mathrm{d}x. \tag{16}$$

It is noted that the first term of Eq. (16) represents strain energy due to axial deformations including the coupling between axial and bending deformations, which accounts for the geometric nonlinearity. Eq. (16) can be written in compact matrix form as

$$U = \frac{1}{2}\mathbf{e}^{\mathrm{T}}\mathbf{K}\mathbf{e}, \tag{17}$$

where $\mathbf{K}$ is the augmented stiffness matrix given by $\mathbf{K} = \mathbf{k}_a + \mathbf{k}_b + \mathbf{k}_\varphi + \mathbf{k}_{as}$, where $\mathbf{k}_a$ is the axial stiffness matrix, $\mathbf{k}_b$ is the bending stiffness matrix, $\mathbf{k}_\varphi$ is the torsional stiffness matrix, and $\mathbf{k}_{as}$ is the axial stiffening matrix due to the gravitational field, which accounts for the stiffening effect on the tension field and the softening effect on the compression field of the drillstring. These coefficient matrices are given by

$$\mathbf{k}_a = \mathbf{k}_1 - \mathbf{k}_2 - \mathbf{k}_3 - \mathbf{k}_4, \quad \mathbf{k}_b = \int_0^l \mathbf{B}_\theta^{\mathrm{T}} EI\mathbf{B}_\theta \,\mathrm{d}x, \quad \mathbf{k}_\varphi = \int_0^l \mathbf{B}_\varphi^{\mathrm{T}} GI_p\mathbf{B}_\varphi \,\mathrm{d}x, \quad \mathbf{k}_{as} = \int_0^l F\mathbf{B}_v^{\mathrm{T}}\mathbf{B}_v + \mathbf{B}_w^{\mathrm{T}}\mathbf{B}_w^{\mathrm{T}} \,\mathrm{d}x,$$

where

$$\mathbf{k}_1 = \int_0^l \mathbf{B}_u^{\mathrm{T}} EA\mathbf{B}_u \,\mathrm{d}x, \quad \mathbf{k}_2 = \int_0^l \frac{3}{2}EA\mathbf{B}_u^{\mathrm{T}}\mathbf{B}_u\mathbf{e}\mathbf{B}_u \,\mathrm{d}x, \quad \mathbf{k}_3 = \int_0^l EA\left(\frac{1}{2}\mathbf{B}_u^{\mathrm{T}}\mathbf{B}_{\theta_y}\mathbf{e}\mathbf{N}_{\theta_y} + \mathbf{N}_{\theta_y}^T\mathbf{B}_u\mathbf{e}\mathbf{B}_{\theta_y}\right) \mathrm{d}x,$$
$$\mathbf{k}_4 = \int_0^l EA\left(\frac{1}{2}\mathbf{B}_u^{\mathrm{T}}\mathbf{B}_{\theta_z}\mathbf{e}\mathbf{B}_{\theta_z} + \mathbf{B}_{\theta_z}^{\mathrm{T}}\mathbf{B}_u\mathbf{e}\mathbf{B}_{\theta_z}\right) \mathrm{d}x.$$

2.3. Stick–slip model

In order to understand the stick–slip phenomenon, some mathematical models were proposed to simulate the drillstring dynamics under various conditions. Both analytical and numerical approaches were employed to describe the BHA movement. Some common difficulties associated with the existing models have lead to inconsistency with field data. One of the major problems is the inaccurate description of some of the involved parameters and/or downhole boundary conditions, which affect the model. Moreover, the dynamic modeling of the stick–slip phenomenon is a challenging problem because the presence of static and kinetic friction mechanisms leads to discontinuous differential equations [6].

It is known that the friction force is responsible of the self-excited stick–slip phenomenon. Accordingly, an accurate stick–slip model must account for the parameters that affect the friction mechanism; such as angular displacement, and angular velocity. The initial value of may be represented by $W_o + k_f x_o$, which after one revolution, is reduced to its constant value W_o as the term $k_f x_o$ vanishes. Since it is consequential to assume that the oscillates harmonically about its mean value W_o, one can express it in the form [14,20]

$$WOB = W_o + k_f x_o(1 - \sin 2\pi f t), \tag{18}$$

where f is the frequency of the fluctuations of, and x_o is the depth of cut in one bit revolution. The frequency f is related to the depth of cut x_o and the rate of penetration (ROP) $\dot{x}$, as $f = \dot{x}/x_0$. The amplitude of the

fluctuating part of the depends on the depth of cut, while the frequency f, of a bit rotating at angular velocity $\dot{\varphi}_o$ and traveling at axial velocity $\dot{x}$, can be calculated from [33]

$$(\text{time})_{\text{rotational motion}} = (\text{time})_{\text{axial motion}}, \text{ i.e. } \frac{2\pi}{\dot{\varphi}_o} = \frac{x_o}{\dot{x}}. \tag{19}$$

Accordingly, in this case, the term $2\pi ft$ in Eq. (18) represents the torsional degree of freedom φ.

In this analysis, it is assumed that the bit never loses contact with the formation. In addition, it is assumed that the bit is constrained in the lateral direction. In order to include the effect of axial motion on the torsional oscillations, the coupling between axial degree of freedom and angular velocity is introduced in defining the torque term. As a result, torque-on-bit (TOB) is assumed to be dependent on, as

$$\text{TOB} = \mu_k W \xi(\dot{\varphi}), \tag{20}$$

where μ_k is the coefficient of kinetic friction, and the torque in Eq. (20) becomes $\text{TOB} = \text{TOB}(\varphi, \dot{\varphi})$. The function $\xi(\dot{\varphi})$ relates TOB to the angular velocity of the bit. For angular speeds relevant to typical oil drilling operations, a friction profile that accommodates the expected variation of the friction torque as a function of angular velocity was adopted by several investigators [6,11,18]. Some other investigators used characteristics curves to model this relation [12,32]. However, experiments and field data records showed that the applied friction torque is proportional to the high fluctuations in the bit angular velocity. Unfortunately, there is no field data available to describe this relation at low velocities, and engineers usually perform extrapolation to plot the curve at low velocities. The concern about low velocity region relates to the fidelity of the stick–slip model at the region of transition from static to kinetic friction. However, at high velocities, all functions adopted in the aforementioned previous investigations tend to converge to a constant value.

In general, the adopted functions of $\xi(\dot{\varphi})$ may be classified as either continuous or discontinuous functions. The discontinuity in some proposed expressions posses a major source of computational difficulty, when it comes to numerical integration. A smooth representation of $\xi(\dot{\varphi})$ over the short-lived transition event was adopted by several investigations, and was found to be rather accurate and computationally more efficient [16]. A continuous representation of $\xi(\dot{\varphi})$, similar to the one adopted in Ref. [16], is given by Eq. (21) and employed in this investigation

$$\xi(\dot{\varphi}) = \tanh(\dot{\varphi}) + \frac{\alpha_1 \dot{\varphi}}{1 + \alpha_2 \dot{\varphi}^2}. \tag{21}$$

2.4. Equations of motion

By utilizing the above energy expressions into the variational form of Lagrange equation, and using the standard finite element assembly procedure, the equation of motion of the drillstring can be written in the assembled general form as

$$\mathbf{M}\ddot{\mathbf{e}} + \mathbf{G}\dot{\mathbf{e}} + \mathbf{K}\mathbf{e} = \mathbf{Q}, \tag{22}$$

where $\mathbf{M}$ is the global assembled mass matrix of the system, $\mathbf{G}$ is the gyroscopic matrix of the system, $\mathbf{K}$ is the global assembled stiffness matrix of the system, $\{e\}$ is the deformation vector, and $\mathbf{Q}$ is the generalized force vector that accommodates the nonlinear inertia coupling terms, the TOB and other external excitations. The mass matrix $\mathbf{M}$ and the stiffness matrix $\mathbf{K}$ are symmetric, while the gyroscopic matrix $\mathbf{G}$ is skew-symmetric. The developed elastodynamic model does not account for damping. It is noteworthy to mention that damping is an important aspect to the dynamic behavior of drilling systems. In drilling applications, damping arises from structural material damping and viscous damping due to drilling mud interaction with the rotating drillstring. Adding structural material damping is a straightforward task, and is often accounted for by an assumed linear model in the form of proportional modal damping [27], yet the elements of such damping matrices are merely rough estimates. Accordingly, adding damping may overshadow the clarity of insight gained by examining the undamped system. However, viscous damping due to drilling fluid–structure interaction is more significant, and must be taken into account in a more comprehensive dynamic model. Studying the dynamics of drillstrings in the presence of mud flow represents a problem of continued interest by

some investigators. Few attempts to tackle this problem, both analytically and experimentally, have been reported [28,39,40].

3. The reduced-order model

In order to obtain the solution of the generalized eigenvalue associated with the homogenous equation of motion, one can represent Eq. (22) in the following state-space form [36,37]

$$\mathbf{A}\dot{\mathbf{y}} + \mathbf{B}\mathbf{y} = \bar{\mathbf{Q}}, \tag{23}$$

where for constant rotational speed of the drillstring, the coefficient matrices of Eq. (23) are given bywhere for constant rotational speed of the drillstring, the coefficient matrices of Eq. (23) are given by

$$\mathbf{A} = \begin{bmatrix} \mathbf{0} & -\mathbf{M} \\ \mathbf{M} & \mathbf{G} \end{bmatrix}, \quad \mathbf{B} = \begin{bmatrix} \mathbf{M} & \mathbf{0} \\ \mathbf{0} & \mathbf{0} \end{bmatrix}, \quad \mathbf{y} = \begin{Bmatrix} \dot{\mathbf{e}} \\ \mathbf{e} \end{Bmatrix}, \quad \bar{\mathbf{Q}} = \begin{Bmatrix} \mathbf{0} \\ \mathbf{Q} \end{Bmatrix}.$$

The dimension of each of the matrices **M**, **K** and **G** is $(6n \times 6n)$, where n is the number of nodes, while the matrices **A** and **B** are of dimension $(12n \times 12n)$.

In order to obtain the reduced order modal form, let **R** and **L** denote the right and left complex modal transformation matrices, respectively, which are associated with the differential operators of Eq. (14). Now, one can introduce the modal transformation $\mathbf{y} = \mathbf{R}\mathbf{u}$, where **u** is the vector of modal coordinates. In general, the modal matrices **R** and **L** are composed of a set of complex eigenvectors (mode shapes) that account for a selected set of significant modes. Pre-multiplying both sides of Eq. (23) by $\mathbf{L}^{\mathrm{T}}$ and substituting for **y** in terms of modal coordinates **u**, the truncated modal form of the equations of motion can be written as

$$\mathbf{A}_r\mathbf{u} + \mathbf{B}_r\mathbf{u} = \mathbf{Q}_r, \tag{24}$$

where $\mathbf{A}_r = \mathbf{L}^{\mathrm{T}}\mathbf{A}\mathbf{R}$ and $\mathbf{B}_r = \mathbf{L}^{\mathrm{T}}\mathbf{B}\mathbf{R}$ represent the reduced modal matrices, while $\mathbf{Q}_r = \mathbf{L}^{\mathrm{T}}\bar{\mathbf{Q}}$ is the reduced modal forcing vector.

4. Numerical results

A computational scheme is developed based on the presented formulation using MATLAB$^{\mathrm{TM}}$. The presence of damping is known to stabilize the numerical integration. Although, damping is not present in this model, the integration scheme adopted herein is a high-order predictor-corrector algorithm with adaptive step size and optimized error control, which functions perfectly well even for undamped systems. In this numerical demonstration, a drillstring of the specifications adopted in Ref. [13] and given in Table 1 is considered. The results are obtained using the consistent mass FEM formulation with 24 finite shaft elements. This number of elements was found to achieve convergence for the chosen drillstring configuration. Numerical tests showed

Table 1
Drillstring data

Drillpipe specification	
Drillpipe length	1000 m
Drillpipe outer diameter	0.127 m
Drillpipe inside diameter	0.095 m
Drillcollar specification	
Drillcollar length	200 m
Drillcollar outer diameter	0.2286 m
Drillcollar inside diameter	0.0762 m
Material specification	
Drillstring density	7850 kg/m^3
Modulus of elasticity	210×10^9 N/m^2
Shear modulus	7.6923×10^{10} N/m^2

that further increase of number of elements resulted in insignificant improvement in the calculated values. A total of 140 degrees of freedom is retained after applying the boundary conditions for the drillstring system. The following discussion is primarily meant for a drillstring in vertical borehole where no initial curvature is involved.

4.1. Dynamic response analysis

The capability of the developed computational scheme is now tested for dynamic response calculations. The drillstring transient response is obtained for two different excitations; initial displacement and an applied impulsive force. In order to calculate the transient response of the rotating drillstring due to initial displacement, an admissible displacement field is considered. The initial displacement field is calculated by applying a force at approximately midway of drillpipe and calculating the nodal displacement from the static defection equation. The dynamic response of node 3 is shown in Fig. 3 for both the full-order and the reduced-order models. A fifth-order reduced model is obtained using the aforementioned modal transformation with the first five modes retained as significant modes. It is interesting to observe that a five-DOF reduced model gives a quite satisfactory response to that of 140-DOF full-order model.

The response of the system due to an impulsive excitation is considered by subjecting the drillstring to an initial velocity in the lateral direction of node 10 (the midpoint of the drillpipe). The response of node 3 is shown in Figs. 4 and 5, for two different reduced models. It is well-known in impact dynamics [38] that impulsive forces tend to excite higher frequencies, thus engaging higher modes to share an appreciable amount of the system's kinetic energy. Consequently the reduced-order model needs to be expanded to include more significant modes. The 8-DOF reduced-order model in Fig. 5 is shown to approach the full-order solution more accurately than the 5-DOF model.

4.2. Dynamic response due to coupling

Secondly, the developed scheme is used to demonstrate the effect of coupling between axial–torsional–lateral structural vibrations of the drillstring. Coupling could be a potential source of ambiguous vibrations in drillstrings. It is essential to consider coupling while simulating real drilling systems in order for the model to adequately acquire a realistic insight of their dynamic behavior. In this numerical simulation, the time responses of the drillstring system are evaluated under various lateral excitations to show their effects on axial

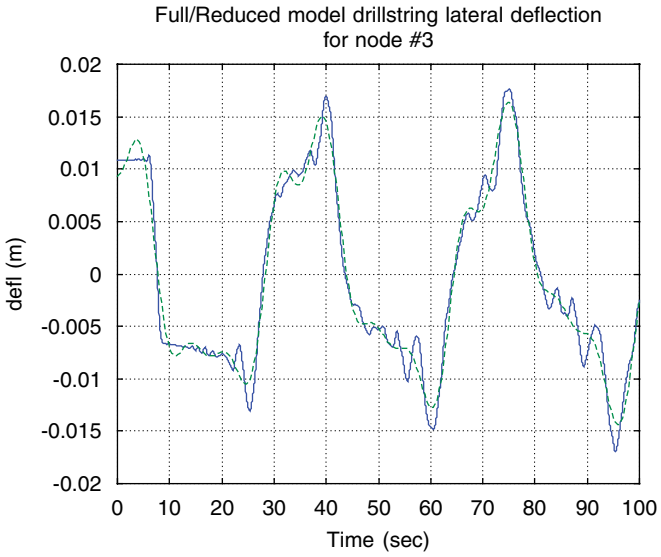

Fig. 3. Transient response of node 3 due to initial displacement input ((▬) full order and (▬) reduced order).

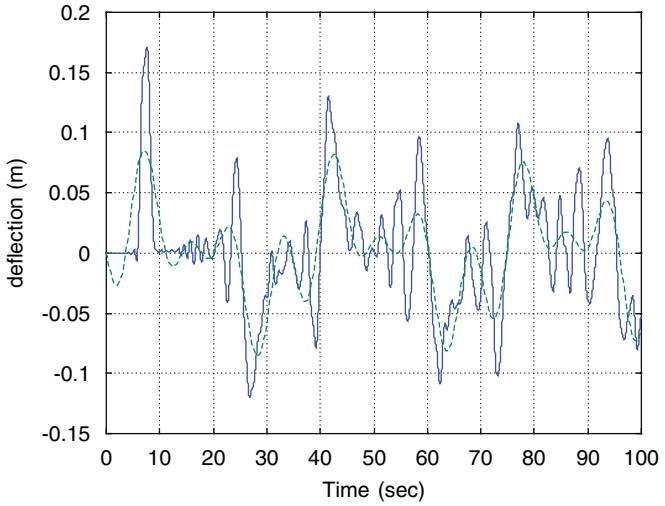

Fig. 4. Transient response of node 3 due to initial velocity ((——) full order and (——) reduced order).

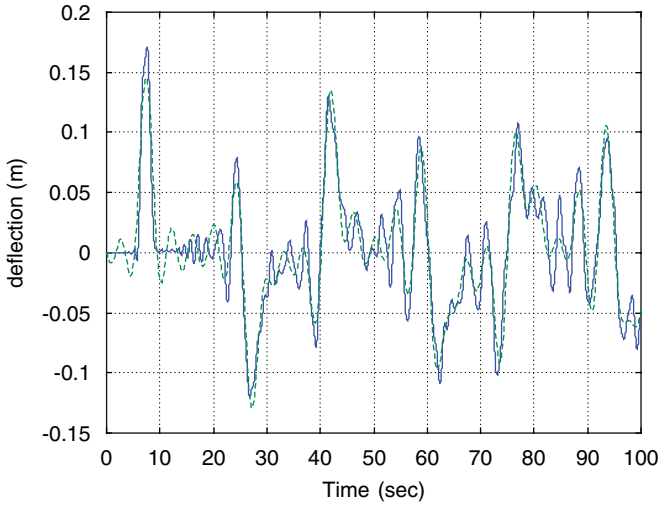

Fig. 5. Transient response of node 3 due to initial velocity ((——) full order and (——) reduced order).

and torsional directions. A 5-DOF reduced order model was employed in this case. Figs. 6–8 show the axial response due to initial displacement, initial velocity and constant force in the lateral direction at node 10 (the midpoint of the drillpipe segment), respectively. In order to examine the severity of transverse excitations on the torsional behavior, several excitations were applied in the lateral direction to observe the consequent torsional response. Figs. 9–11 display the torsional responses, which are solely due to coupling with lateral motion in the absence of any torsional loads. This coupling may become even more significant if large lateral forces due drillstring–borehole interaction, as well as higher values of WOB are encountered in normal drilling operations.

4.3. Stick–slip self-excited response

It has been established that friction torque is responsible for the severe stick–slip vibrations in drillstrings. To obtain the drillstring response due to friction torque excitation, an appropriate torque term is included in

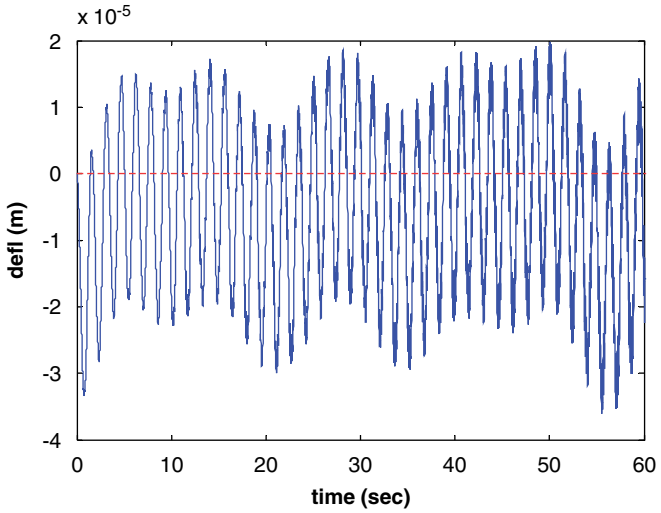

Fig. 6. Axial deflection due to lateral initial displacement.

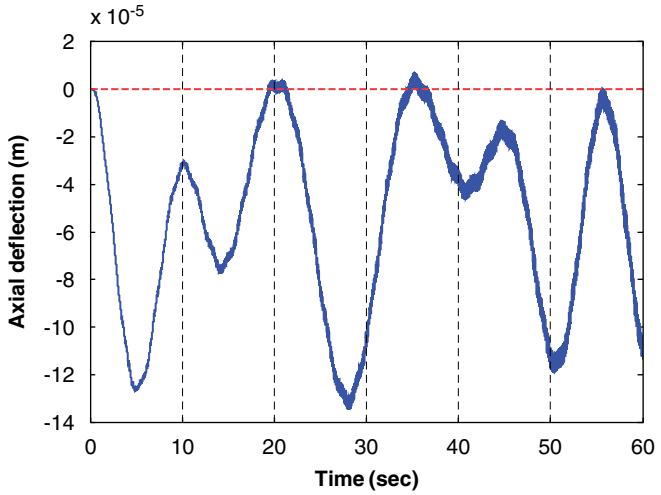

Fig. 7. Axial deflection due to lateral velocity.

the forcing vector of the governing equation. The parameters used in this simulation represent a typical case in oil well drilling operations, and are given by $W_0 = 100\,\text{kN}$, $k_f = 25{,}000\,\text{kN/m}$, $x_o = 0.001\,m$, $\mu_k = 0.04$, $\alpha_1 = 2$, and $\alpha_2 = 1$. Figs. 12 and 13 show the drillstring angular speed at the surface (rotary table) and at 200-m above the bit, respectively. Fig. 14 shows the instantaneous bit angular speed over a period of 20 s of fully developed stick–slip while drilling. The mean angular speed of the rotary table is 110 rev/min (10.5 rad/s), which is constant over time while the bit is oscillating between a complete standstill, and a very high velocity that reaches about three times the surface velocity. This is in agreement with field measurements, which have shown that when there are significant torsional vibrations, the bit speed differs from the rotary table speed by as much as three times, as reported by previous investigations [13].

Another important parameter to be investigated in stick–slip problems is the developed torque profile. The fluctuations of torque could be very detrimental to the drilling bit and downhole equipment. Typical torque evolution during stick–slip oscillation is shown in Fig. 15. During slip phase, there are periodic fluctuations in the torque profile around the mean value 5000 N m. The amplitude of this fluctuation is relatively small but the

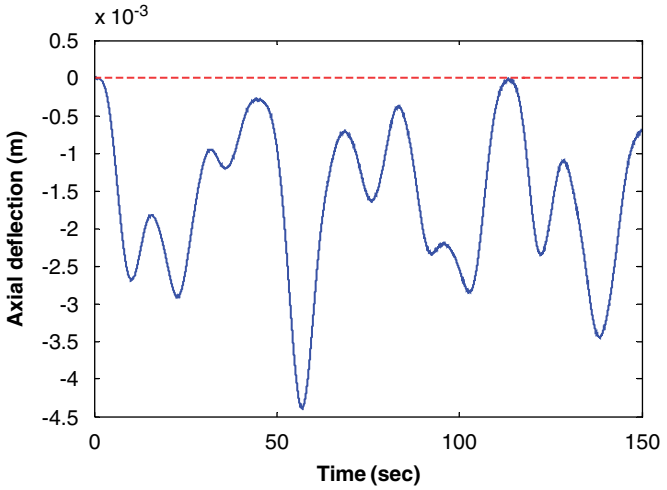

Fig. 8. Axial deflection due to lateral constant force.

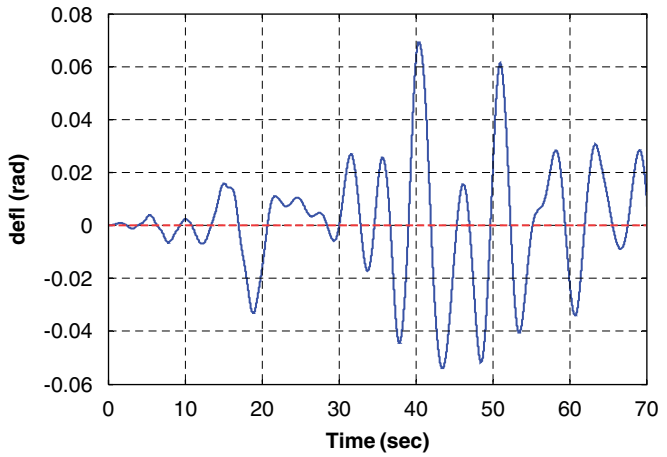

Fig. 9. Torsional response due to lateral initial displacement.

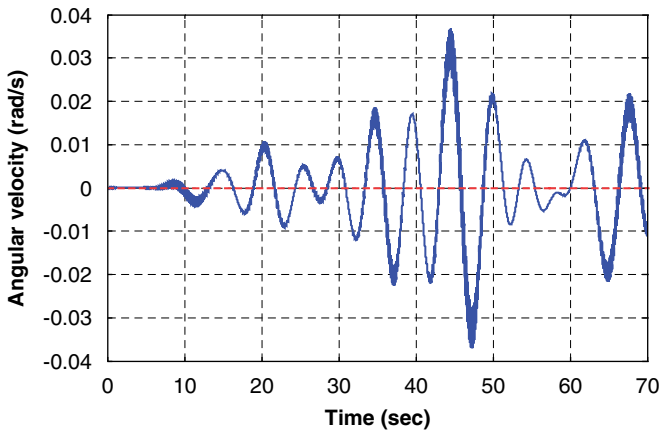

Fig. 10. Torsional response due to lateral initial velocity.

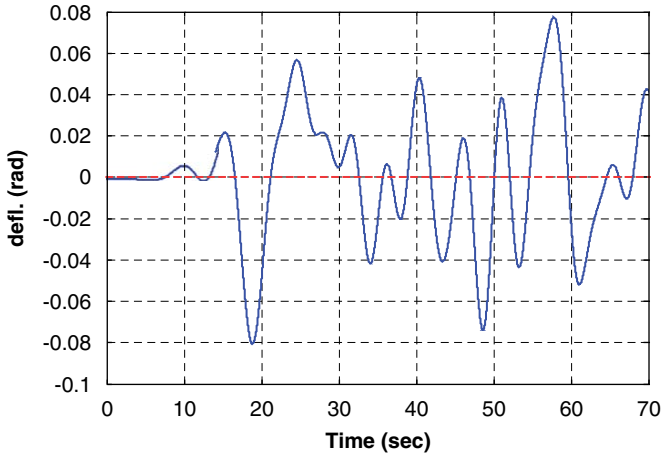

Fig. 11. Torsional response due to lateral constant force.

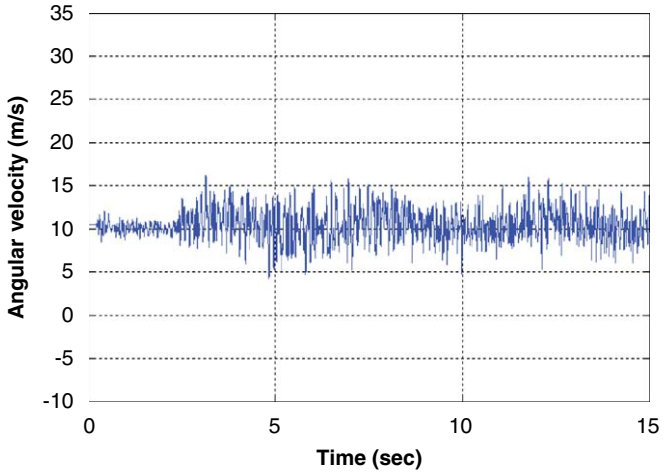

Fig. 12. Torsional stick–slip oscillation at the rotary table.

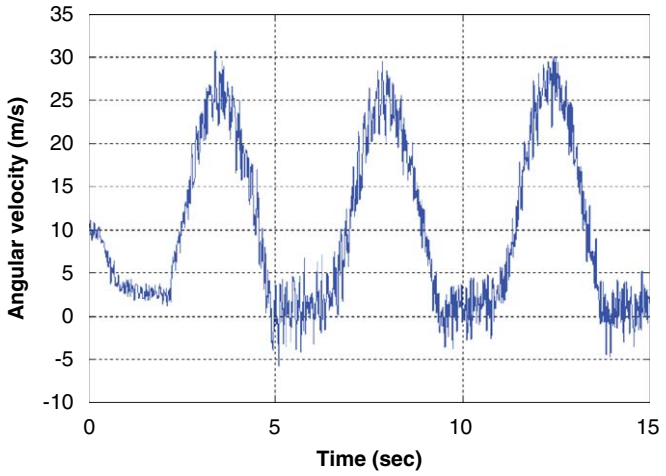

Fig. 13. Torsional stick–slip oscillation at 200-m above the bit.

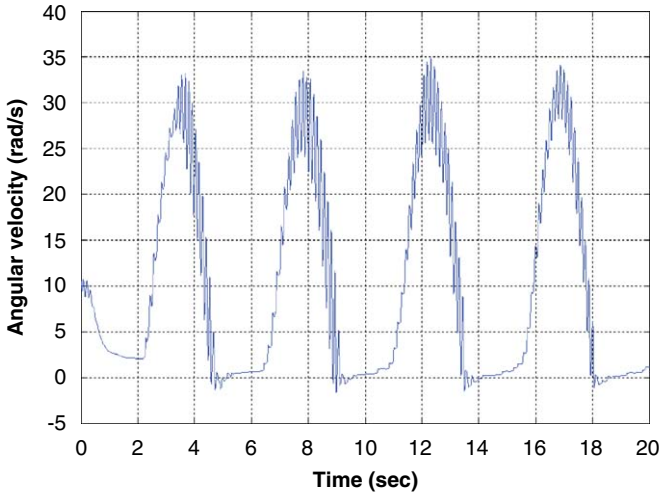

Fig. 14. Torsional stick–slip oscillation at the drilling bit.

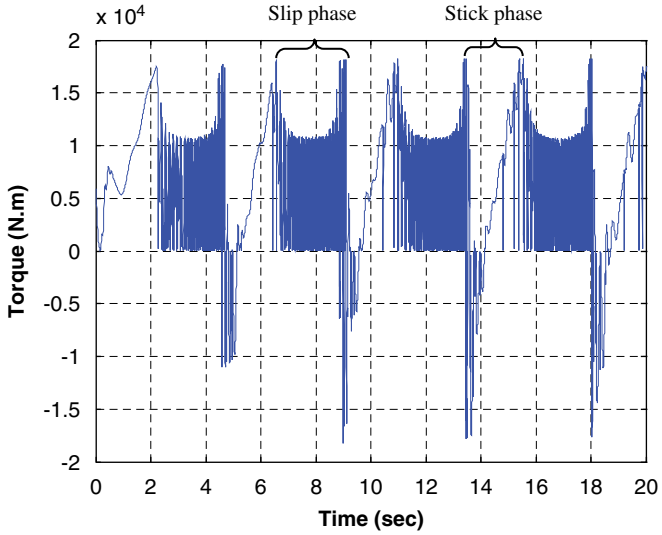

Fig. 15. Torque on bit profile for stick–slip oscillations (full-order model).

fluctuation frequency is high. Suddenly, the toque mean value drops to minimum value, which indicates that the bit is about to stick. In the stick regime, the bit momentarily stops causing the top torque and TOB to build up in almost linear fashion to reach very large value.

Stick–slip oscillation as experienced in drilling process is an example of limit-cycling behavior [13]. To demonstrate this behavior, the trajectory of the bit displacement relative to the rotary table versus the bit instantaneous velocity is obtained in Fig. 16. The initial bit speed is 110 RPM which is same as rotary speed. A straight line at zero speed represents the stick phase. During slip phase, the velocity increases while the displacement returns back to its equilibrium position. In Fig. 16, the zero value on the displacement axis represents the location of the rotary table. The region to the left side of this point (negative displacement) implies that bit is lagging behind the rotary table. Positive values of the displacement indicate that the bit is leading the rotary table at this region; i.e. the instantaneous speed of the bit is greater than the rotary speed.

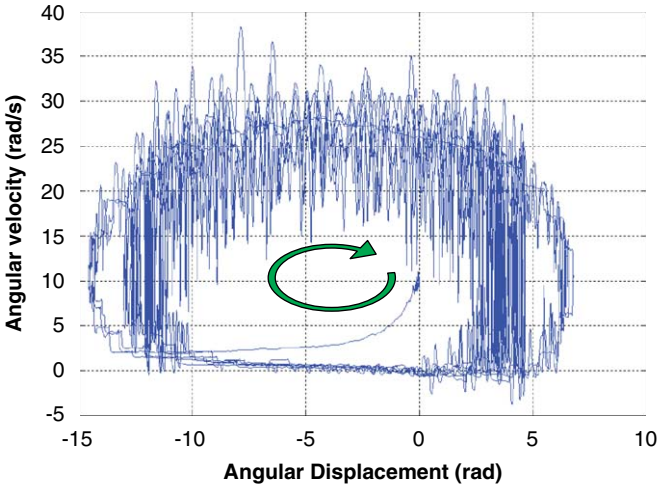

Fig. 16. Phase plane of the bit during stick–slip oscillations (full-order model).

5. Conclusions

A finite element dynamic formulation of the vibrational characteristics of rotating drillstring is developed. The model accounts for the gyroscopic, as well as the axial/bending, bending/torsional coupling, and the stick–slip interaction. In addition, the axial gravitational filed effect on the drillstring, which was ignored by other FEM formulations, has been considered. Complex modal transformations are applied and reduced-order models are obtained. The finite element formulation is then integrated into a computational scheme for calculating the natural frequencies of the whole drillstring. The computational scheme is extended further to integrate the equations of motion, either in the full-order or the reduced-order form, to obtain the dynamic response. Numerical demonstrations using different excitations are considered to validate the model, and some benchmark solutions are presented. The results obtained are in excellent agreement with actual field observations and measurements.

The method developed in this paper is intended to furnish the basic building block for further development of more comprehensive drilling assembly models that can easily accommodate other related dynamic effects resulting from wellbore/drillpipe contact and drillstring/mudflow interaction. Research is currently underway by the authors, both analytically and experimentally, to extend the developed model to include the related dynamic effects of string/borehole interaction and the effect of damping due to the drilling mud flow.

Acknowledgment

This research work is funded by King Abdulaziz City for Science & Technology; KACST Project No. AR-22-11. The authors greatly appreciate the support provided by KACST and King Fahd University of Petroleum & Minerals during this research.

References

[1] J.J. Bailey, I. Finnie, An analytical study of drillstring vibration, *Journal of Engineering for Industry, ASME Transaction* 82 (2) (1960) 122–128.

[2] I. Finnie, J.J. Bailey, An experimental study of drillstring vibration, *Journal of Engineering for Industry, ASME Transaction* 82 (2) (1960) 129–135.

[3] D.W. Dareing, B.J. Livesay, Longitudinal and angular drillstring vibrations with damping, *Journal of Engineering for Industry, ASME Transaction* November (1968) 671–679.

[4] L.F. Kreisle, J.M. Vance, Mathematical analysis of the effect of shock sub on the longitudinal vibrations of an oilwell drillstring, *SPE* December (1970) 349–356.
[5] I.G. Eronini, W.H. Somerton, D.M. Auslander, A dynamic model for rotary rock drilling, *Energy Resources Technology* June (1982) 108–120.
[6] R.I. Leine, D.H. Van Campen, L. van den Steen, Stick–slip vibrations induced by alternate friction models, *Nonlinear Dynamics* 16 (1998) 41–54.
[7] G.w. Halsey, A. Kyllingstad, T.V. Aarrestad, D. Lysne, Drillstring torsional vibrations: comparison between theory and experiment on a full-scale research drilling rig, *SPE 15564*, *Proceedings of the SPE Annual Technical Conference and Exhibition*, New Orleans, October 5–8, 1986.
[8] A. Kyllingstad, G.W. Halsey, A study of slip/stick motion of the bit, *SPE 16659*, *Proceedings of the 62nd Annul Technical Conference of the SPE*, Dallas, TX, September 27–30, 1987.
[9] N. Challamel, E. Sellami, E. Chenevez, L. Gossuin, A stick–slip analysis based on rock/bit interaction: theoretical and experimental contribution, *SPE 59230*. Presented at the *IADC/SPE Drilling Conference*, Orleans, LA, 2000.
[10] R. Dawson, Y.Q. Lin, P.D. Spanos, Drillstring stick–slip oscillations, *Proceedings of the Spring Conference of the Society for Experimental Mechanics*, Houston, TX, 1987.
[11] Y.Q. Lin, Y.H. Wang, Stick–slip vibration of the drill strings, *Journal of Engineering for Industry, ASME Transaction, Series B* 113 (1991) 38–43.
[12] J.F. Brett, The genesis of bit-induced torsional drill string vibrations, *SPE 21943*, *Proceedings of the SPE/IADC Drilling Conference*, Amsterdam, March 11–14, 1991.
[13] J.D. Jansen, L. van den Steen, Active damping of self-excited torsional vibration in oil well drillstrings, *Journal of Sound and Vibration* 179 (1995) 647–668.
[14] T. Richard, E. Detournay, Stick–slip vibrations of PDC bits, *Pacific Rocks* (2000) 33–40.
[15] T. Richard, E. Detournay, Self-excited stick–slip vibrations of drill bits, *Comptes Rendus de l Mecanique* 332 (2004) 619–626.
[16] R.W. Tucker, C. Wang, On the effective control of torsional vibrations in drilling systems, *Journal of Sound and Vibration* 224 (1999) 101–122.
[17] A. Leseultre, E. Lamine, A. Jonsson, An Instrumented Bit: A necessary step to the intelligent BHA, *SPE 39341*, *Proceedings of the IADC/SPE Drilling Conference*, Dallas, TX, 1998.
[18] R.I. Leine, D.H. Van Campen, W.J. Keultjes, Stick–slip whirl interaction in drillstring dynamics, *Journal of Sound and Acoustics* 124 (2002) 209–220.
[19] A.S. Yigit, A.P. Christoforou, Coupled axial and transverse vibrations of oilwell drillstrings, *Journal of Sound and Vibration* 195 (4) (1996) 617–627.
[20] A.S. Yigit, A.P. Christoforou, Coupled torsional and bending vibrations of drillstrings subject to impact with friction, *Journal of Sound and Vibration* 215 (1) (1998) 167–181.
[21] R.W. Tucker, C. Wang, An integrated model for drill-string dynamics, *Journal of Sound and Vibration* 224 (1) (1999) 123–165.
[22] K. Millheim, S. Jordan, C.J. Ritter, Bottom-hole assembly analysis using the finite-element method, *SPE paper No. 6057*, 1978, pp. 265–274.
[23] A.A. Besaisow, M.L. Payne, A study of excitation mechanisms and resonances inducing BHA vibrations, *SPE No. 15560*, *Proceedings of the 61st Annual Technical Conference and Exhibition of the Society of Petroleum Engineers*, New Orleans, LA, October 5–8, 1986.
[24] T.M. Burgess, G.L. McDaniel, P.K. Das, Improving BHA tool reliability with drillstring vibration models: field experience and limitations, *SPE 16109, Proceedings of the SPE/ADC Drilling Conference*, New Orleans, LA, March 15–18, 1987.
[25] R.F. Mitchell, M.B. Allen, Case studies of BHA vibration failure, *SPE 16675, Proceedings of the 62nd SPE Annual Technical Conference & Exhibition*, Dallas, TX, September 27–30, 1987.
[26] F.S. Costa, P.R. Rebeiro, Finite Element modeling of the mechanical behavior of unbalanced drillcollars, *SPE 39025, Proceedings of the Fifth Latin American and Caribbean Petroleum Engineering Conference and Exhibition*, Rio de Janeiro, Brazil, August 30–September 3, 1997.
[27] M.C. Apostal, G.A. Haduch, J.B. Williams, A Study to determine the effect of damping on finite-element-based, forced-frequency-response models for bottomhole assembly vibration analysis, *SPE 20458, Proceedings of the 65th SPE Annual Technical Conference and Exhibition*, New Orleans, LA, September 23–25, 1990.
[28] F. Axisa, J. Antunes, Flexural vibrations of rotors immersed in dense fluids: Part I—Theory, *Proceedings of the Third International Symposium on Transport Phenomena and Dynamics of Rotating Machinery*, ISROMAC-3, Honolulu, Hawaii, vol. 2 (2), 1990, pp. 23–38.
[29] V.A. Dunayevsky, F. Abbassian, A. Judzis, Dynamic stability of drillstring under fluctuating weight on bit, *SPE 14329, Proceedings of the SPE Drilling and Completion*, June 1993, pp. 84–92.
[30] A. Berlioz, J. Der Hogopian, R. Dufour, E. Draoui, Dynamic behavior of a drillstring: experimental investigation of lateral instabilities, *Journal of Vibration and Acoustics* 118 (1996) 292–298.
[31] H. Melakhessou, A. Berlioz, G. Ferraris, A nonlinear well-drillstring interaction model, *Journal of Vibration and Acoustics* 125 (2003) 46–52.
[32] B. Schmalhorst, A. Baumgart, Combined simulation of whirl and stick–slip phenomena using a nonlinear finite element model, *Proceedings of the Drilling and Production Engineering Conference*, 1997, pp. 53–60.
[33] N. Challamel, Rock destruction effect on the stability of drilling structure, *Journal of Sound and Vibration* 233 (2) (2000) 235–254.

[34] P. Likens, F. Barbera, V. Baddeley, Mathematical modeling of spinning elastic bodies for modal analysis, *AIAA, Journal* 11 (9) (1973) 1251–1258.
[35] Y.A. Khulief, H. Al-Naser, Finite element dynamic analysis of drillstrings, *Finite Element in Analysis and Design* 41 (2005) 1270–1288.
[36] K.K. Gupta, Eigen-problem solution of damped structural systems, *International Journal of Numerical Methods Engineering* 8 (1974) 877–911.
[37] Y.A. Khulief, M.A. Mohiuddin, On the dynamic analysis of rotors using modal reduction, *Finite Element in Analysis and Design* 26 (1) (1997) 41–55.
[38] Y.A. Khulief, A.A. Shabana, Impact responses in multibody systems with consistent and lumped masses, *Journal of Sound and Vibration* 104 (2) (1986) 187–207.
[39] J. Antunes, F. Axisa, Flexural vibrations of rotors immersed in dense fluids: Part II—Experiments, *Proceedings of the Third International Symposium on Transport Phenomena and Dynamics of Rotating Machinery*, ISROMAC-3, Honolulu, Hawaii, vol. 2 (2), 1990, pp. 39–52.
[40] B. Schmalhorst, Drilling dynamics in the presence of mud flow, *SPE 59236, Proceedings of the IADC/SPE Drilling Conference*, New Orleans, LA, February 23–25, 2000.